Australian Government

Department of Industry, Innovation and Science

Business
Cooperative Research
Centres Program

MONASH University   Civil Engineering

Theory Manual
Module 2 – Pipe failure analysis
Metallic pipe failure analysis

AUTHORS: Guoyang Fu, Benjamin Shannon,
Ravin Deo, Rukshan Azoor, Jayantha Kodikara.
05 / 07 / 2021

QUALITY INFORMATION

Document: Theory Manual, Module 2 – Pipe failure analysis, Metallic pipe failure analysis

Edition date: 05-07-2021

Edition number: 1.1

Prepared by: Guoyang Fu

Reviewed by: Ravin Deo, Benjamin Shannon

Revision history

Revision	Revision date	Details	Revised by
1.1	05-07-21	Updated	Guoyang Fu, Ben Shannon

CONTENTS

ACKNOWLEDGEMENTS

INTRODUCTION

Monash University were tasked to provide lining innovations to enhance market uptake, including a standard and code of practice of use for CIPP liners and spray liners for pressurised pipes in the CRC-project. This was conducted by undertaking literature reviews, field trials, laboratory testing, and numerical modelling. The research findings were implemented into a standard and code of practice for use in the Australian water industry. A decision tool known as the "Monash Pipe Evaluation Platform" was developed to provide guidance to water utilities, applicators and liner manufacturers in the form of an online web-based platform.

The Monash Pipe Evaluation Platform is split into four modules:

1. Pipe ranking

2. Pipe failure analysis

3. Liner selection

4. Lined pipe analysis

Each module provides tools to help the users to make decisions on pipe rehabilitation.

Module 2 – Metallic pipe failure analysis, incorporates the Monash Tool (MT) for pipe stress analysis, remaining life prediction/time to failure and pipe failure probability. The module applies to metallic pipes and was developed specifically for cast iron pipes. The following document examines the theory used for the metallic pipe failure analysis.

1   METALLIC PIPE FAILURE ANALYSIS

Module 2 – Metallic pipe failure analysis, previously known as the Monash Tool (MT), was developed by the Monash Infrastructure Doctors in the Advanced Condition Assessment and Pipe Failure Prediction (ACAPFP) project to facilitate longitudinal failure analysis of buried cast iron pipe barrels with uniform corrosion and/or single corrosion defects that are idealised into ellipsoids.

The pipe failure analysis consists of the following three sub-sections, namely, pipe stress analysis, remaining life prediction/time to failure and pipe failure probability.

1.1   Metallic pipe stress analysis

Most pipes are buried underground (Figure 1) and they deteriorate mostly in the form of corrosion over time. Corrosion of cast iron pipes can generally be classified into uniform and pitting corrosion. Uniform corrosion causes uniform reduction of the pipe wall thickness while pitting corrosion induces localized corrosion pits. Corrosion pits in metals may have various sizes and shapes (ASTM G46-94 2005). Narrow and deep pits (e.g., ratio of length to width is large and angle at the pit bottom is infinitively small) can reasonably be assumed as cracks, the behaviours of which should be described using fracture mechanics concepts (e.g., stress intensity factors) (Anderson 2005). Blunt pits function as stress raisers and intensify the stress field around the pits. This stress intensification caused by blunt corrosion pits is widely known as stress concentration, characterized by stress concentration factors (SCFs) (Pilkey and Pilkey 2008). A large corrosion patch may form from a cluster of small corrosion pits (Figure 2).
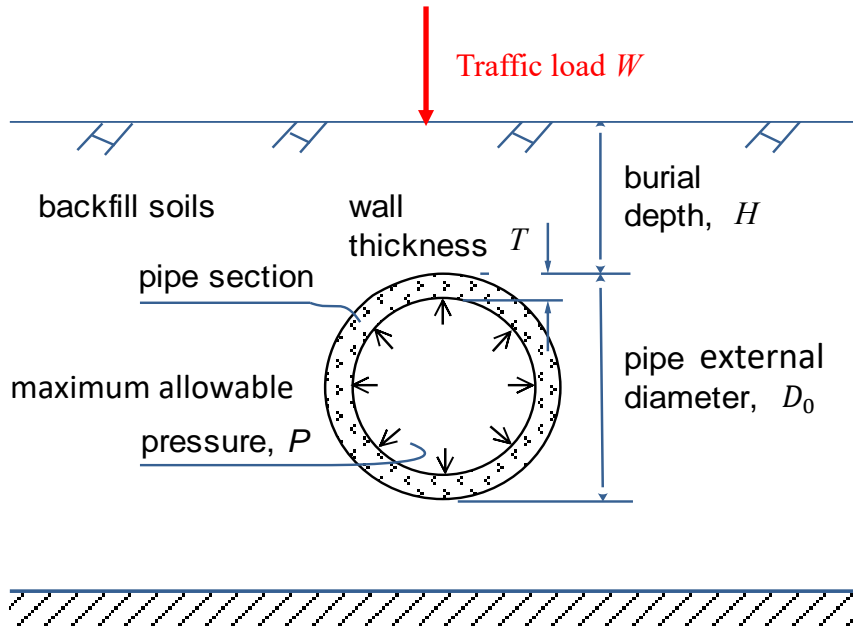
Figure 1. A buried pipe under applied loads

Figure 2. A corrosion patch formed on the external surface of a cast iron pipe

For a buried cast iron pipe with a semi-ellipsoidal corrosion patch on its external surface (Figure 2), the maximum stress σ_{max} in the pipe can be expressed by (Kodikara 2018):

$$\sigma_{max} = \sigma_{nominal} \cdot SCF_{sp} \tag{1}$$

where, $\sigma_{nominal}$ is the nominal stress, and SCF_{sp} is the SCF for the pipe with a surface corrosion patch.

Robert *et al.* (2016) derived an equation to estimate the nominal stress $\sigma_{nominal}$ for an embedded pristine pipe based on finite element analyses given by:

$$\sigma_{nominal} = \frac{W + \gamma_s D_0{}^2 H}{D_0{}^2} \left\{ \xi_1 \left(\frac{E_p}{E_s}\right)^{\psi_1} \left(\frac{E_s}{\gamma_s H}\right)^{\psi_2} \left[\xi_2 \frac{\left(\frac{P}{E_s}\right)^{\psi_3}}{\left(\frac{T}{D_0}\right)^{\psi_4} \left(\frac{W}{\gamma_s D_0{}^2 H} + 1\right)^{\psi_5}} + \xi_3 \frac{\left(\frac{T}{D_0}\right)^{\psi_6} \left(\frac{W}{\gamma_s D_0{}^2 H} + 1\right)^{\psi_7}}{\xi_4 \left(\frac{E_p}{E_s}\right) + \xi_5 \left(\frac{P}{E_s}\right) + \xi_6 \left(\frac{H}{D_0}\right) + \xi_7 k} \right] \right\} \tag{2}$$

where, W is the traffic load (kN), γ_s is the soil unit weight (kN), H is the pipe burial depth (m), E_p and E_s are the modulus of elasticity of the pipe (GPa) and soil (MPa) respectively, P is the internal pressure (kPa), k is the lateral earth pressure coefficient (dimensionless), and ξ and ψ are the coefficients (dimensionless), the values of which are listed in Table 1.

Table 1. Coefficients in Equation (2) (Robert et al. 2016)

Parameter ξ	Value	Parameter ψ	Value
ξ_1	0.12	ψ_1	0.086
ξ_2	4.08	ψ_2	0.94
ξ_3	1.76E+06	ψ_3	0.89
ξ_4	7.65E+04	ψ_4	0.88
ξ_5	4.17E+06	ψ_5	0.94
ξ_6	-3.23E07	ψ_6	-0.51
ξ_7	-3.55E+07	ψ_7	-0.71

For the SCF of surface corrosion patches, Fu *et al.* (2020) derived an equation using non-linear regression based on 456 3D finite element models. The Equation is expressed as follows

$$SCF_{sp} = 1 + \frac{\sqrt[4]{3\left(1 - v_p{}^2\right)}}{2} \left\{ \frac{\alpha_1 \left(\frac{\sqrt{2}a}{\sqrt{D_0 T}}\right)^{\beta_1} + \alpha_2 \left(\frac{\sqrt{2}b}{\sqrt{D_0 T}}\right)^{\beta_2} + \alpha_3 \left(\frac{\sqrt{2}c}{\sqrt{D_0 T}}\right)^{\beta_3}}{\alpha_4 \left(\frac{\sqrt{2}a}{\sqrt{D_0 T}}\right)^{\beta_4} + \alpha_5 \left(\frac{\sqrt{2}b}{\sqrt{D_0 T}}\right)^{\beta_5} + \alpha_6 \left(\frac{\sqrt{2}c}{\sqrt{D_0 T}}\right)^{\beta_6}} \right\} \alpha_7 \left(\frac{c}{T - c}\right)^{\beta_7} \tag{3}$$

where, v_p is the Poisson's ratio of cast iron, α_i and β_i (i = 1-7) are the coefficients, the values of which are given in Table 2.

Table 2. Values of the coefficients α and β in Equation (3)

Parameter α	Value	Parameter β	Value
α_1	2.34E-08	β_1	1.017
α_2	1.57E-07	β_2	1.327
α_3	0.5	β_3	30.788
α_4	3.26E-09	β_4	1.375
α_5	1.43E-06	β_5	1.114
α_6	0.043	β_6	45.635
α_7	17.492	β_7	0.454

It should be noted that the "Remaining life prediction/Time to failure" (Section 1.3) is limited to be valid within the range of variables for buried pipes, as listed in Table 3, where the units for each input variable are given. It can be applied for variables outside these limits, albeit the results have to be checked. Thermal stress due to temperature changes is not considered in the "Remaining life prediction/Time to failure" (Section 1.3).

Table 3. Physical properties for large-diameter cast iron buried pipes

Description of physical parameters		Symbol	Unit	Value for NLR[*]
Location	Burial depth	H	mm	300, 800, 1300, 2000
Backfill soil surrounding pipelines	Elastic modulus	E_s	MPa	2, 4, 10, 25, 50
	Unit weight	γ_s	kN/m^3	18.5
	Lateral earth pressure coefficient	k		0.1, 0.25, 0.4
	Poisson's ratio	ν_s		0.3
Pipe physical properties (cast iron)	Elastic modulus	E_p	GPa	100
	Poisson's ratio	ν_p		0.3
	Wall thickness	T	mm	4, 8, 10, 15, 27
	Internal diameter	D	mm	300, 660, 1000
Load	Traffic load	W	kN	0 to 75
	Maximum allowable pressure	P_{max}	kPa	0, 300, 500, 800, 1000, 1300, 1500

[*] Values used in conducting the non-linear regression analysis.

The following should also be noted:

- The calculated SCF in the pipe stress analysis considers the influence of a 2nd small corrosion defect that is hardly detectable at the bottom of a primary corrosion patch/pit. Our numerical findings demonstrated that 1) the 2nd defect can cause a significant higher value of the SCF; 2) simply increasing the depth of the primary corrosion patch/pit to account for the depth of 2nd defect is found to result in an underestimate of the actual impact of the 2nd pit. For practical purposes, a factor of 1.5 of the SCF based on a series of preliminary numerical investigation is incorporated in the calculation of the SCF. However, the influence is dependent on the size and depth of the 2nd defect.

- An in-situ irregular corrosion defect needs to be idealised into an equivalent ellipsoid (or crater) shape, and the corrosion depth *c* is the maximum corroded depth within the corrosion defect, as shown in Figure 3. This methodology is similar to the procedure given in ASME B31 (2012), but has been checked by Monash Infrastructure Doctors for applicability to water pipes. For details of the checking, please refer to Fu *et al.* (2020) and Zhang *et al.* (2017).
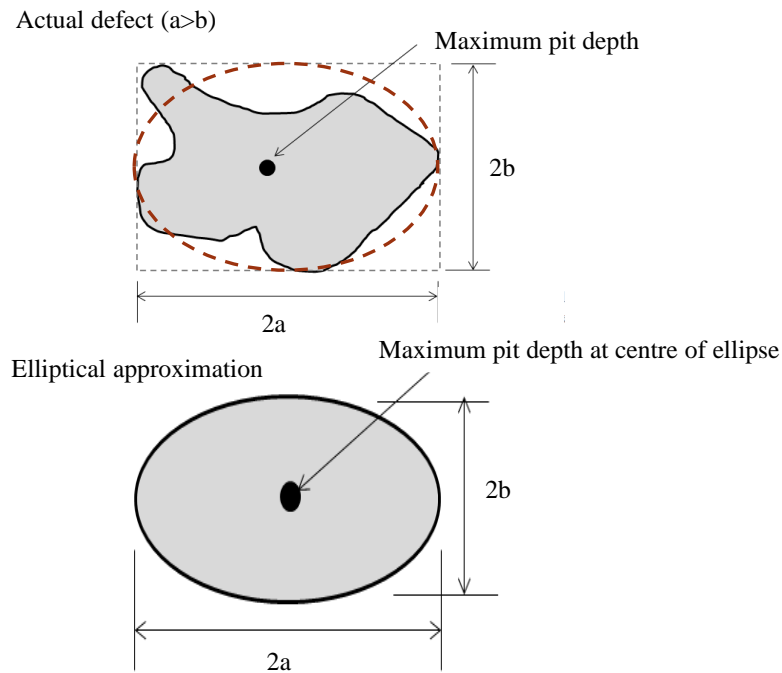
Actual defect (a>b)

Maximum pit depth

2a

2b

Elliptical approximation

Maximum pit depth at centre of ellipse

2a

2b

Figure 3. Approximation of an irregular corrosion geometry by an ellipsoid

- For an oriented corrosion defect, the length $2a$ varies as per the changes of the orientation angle, θ, as indicated in Figure 4. This methodology was adopted from ASME B31 (2012), and has been checked by Monash Infrastructure Doctors for applicability.

$2a_1$

Use $a=a_1$ **for angle ≤ 45 deg** to pipe axis; b remains unchanged

$2b$

θ

Use $a=a_2$ **for angle > 45 deg** to pipe axis; b remains unchanged

$2a_2$
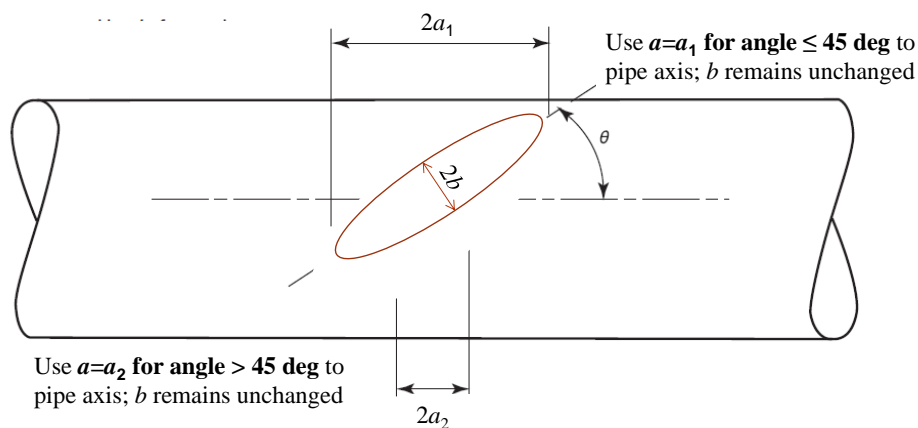
Figure 4. Change of length, $2a$, for an oriented corrosion defect

It is expected that fracture initiation may lead to a "LEAK". However, in reality, whether a leak will occur or not would depend on the length of the crack generated through initial failure. For small pits, pit basal failures will mean the creation of through-wall holes and a leak may or may not be detectable in these through-wall holes due to cement lining and/or graphitisation slowing/inhibiting leak rates. For larger patches, however, a larger crack may be generated, which can lead to leakage. For large patches with a flat bottom, a transition from leak before break may not be present causing a sudden pipe burst without warning.

A general flow chat of the pipe stress analysis in the pipe evaluation platform is shown in Figure 5.

Option 2

Scanned Thickness Maps (CSV file)

Patch Identification algorithm

Option 1

Manual input of patches (single or multiple)

Corrosion Patch $(2a, 2b, c)$

Identified patches

Corrosion Patch 1 $(2a_1, 2b_1, c_1)$,

Corrosion Patch 2 $(2a_2, 2b_2, c_2)$,

$\vdots$

Corrosion Patch n $(2a_n, 2b_n, c_n)$.

Pipe stress analyses

Other input parameters (Pipe properties, soil properties and loading conditions)

Patch Stress Analysis Result (Output)

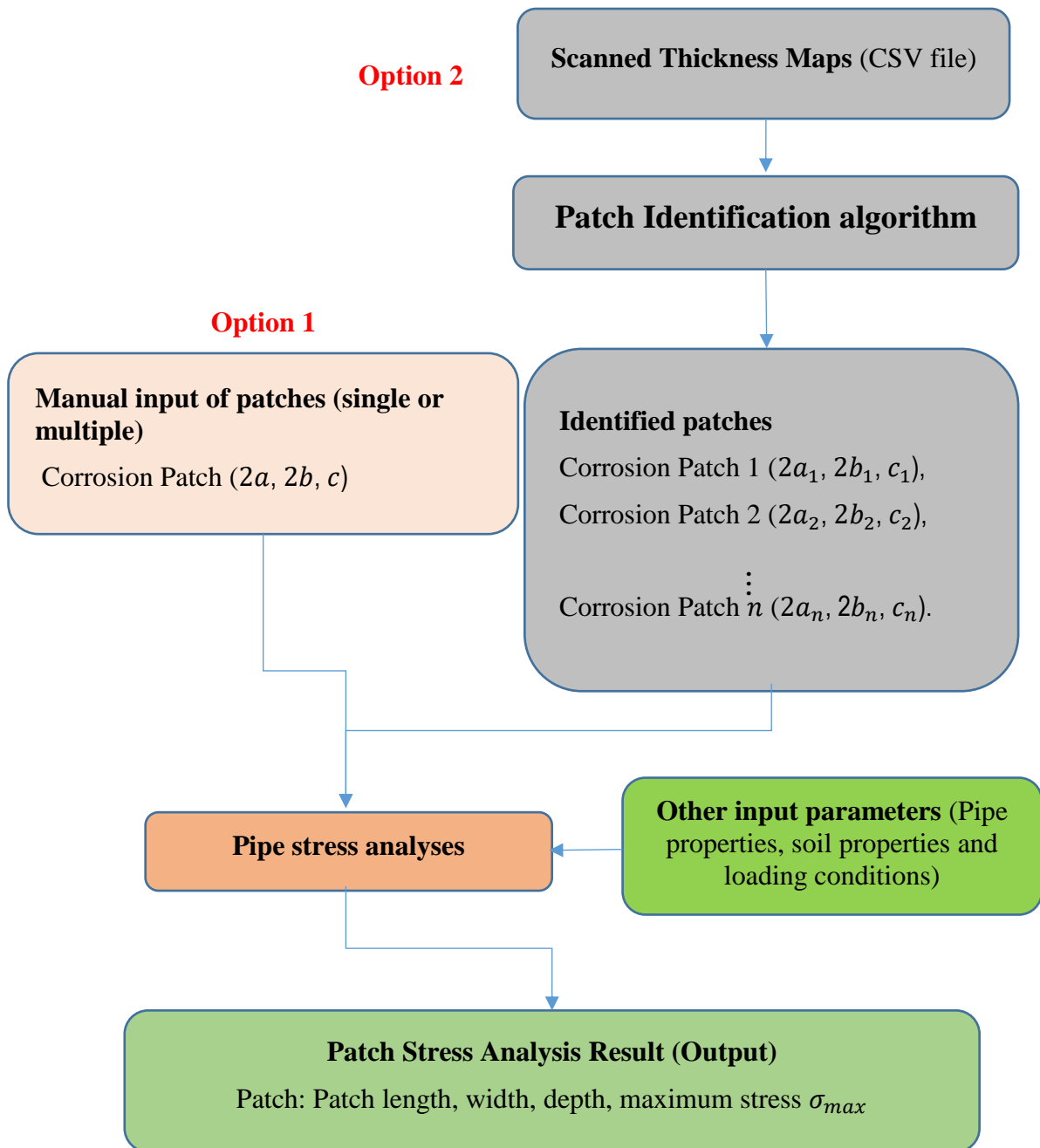Patch: Patch length, width, depth, maximum stress σ_{max}

Figure 5. Flow chart for the pipe stress analysis

1.2   Patch identification algorithm based on scanned wall thickness maps

Emergence of (large) corrosion patches in old cast iron pipes are common and Monash has developed a working definition of the corrosion patches (Deo *et al.* 2019). The definition acknowledges the random nature of corrosion patches and was derived based on observations made on high-resolution (1 mm × 1 mm) scans of old cast iron pipes. The reader is directed to the paper for a detailed discussion on the random geometries of corrosion patches. Section 1.1 and further research was conducted to compare the maximum stresses on pipes based on 1) actual pipe scans with random defects and 2) approximated elliptical corrosion patches segmented from the pipe scans. Results indicate that the maximum stresses computed using both approaches are relatively consistent and therefore the reduction of random corrosion patch geometries into elliptical geometries are appropriate for structural integrity analysis.

The problem

The pipe scans, acquired using a pipe wall-thickness scanner (such as laser scanner, pulse eddy current, etc.), are used for segmenting elliptical corrosion patches to determine their dimensions (length $2a$, width $2b$, depth c), which are subsequently used in Section 1.1 for stress analysis. Some pipe wall-thickness scans are low-resolution pipe scans (*e.g.*, 12.5 mm × 30 mm). A practical approach taken to identify patches in pipe scans involves thresholding pit depths below a certain level in order mask them. The threshold level, usually expressed as a percentage of wall loss, used has always been a matter of discussion as it is based on an estimate of the uniform level of corrosion observed in the pipe scan, requires expert analysis, and can be analyst dependent. Therefore, a systematic procedure is required that can remove the analyst dependency and lead to an analytical procedure for segmenting elliptical corrosion patches, which is also currently sought by UTS for analysis of their wall thickness realisations. Data was gathered from pipe scans of Sydney Water pipes.

A solution

The pit depth data in a pipe scan will usually exhibit a normal distribution as schematised in Figure 6. Although the origin of these pits can be attributed to various factors, they can be grouped within 3 classes; low, average, and high damages to indicate the degree of corrosion rate causing them to manifest. It is important to note that these classifications are not based on time only, but also the severity of the corrosion attack. For example, a 40-year old pipe can suffer extensive corrosion damage over a short (*e.g.*, 5 year) period at a localised region within the pipe scan area, with the maximum pit depth manifesting within this period, while other pipe scan regions can be corroding slowly over longer periods. Nevertheless, the presence of a normally distributed pit depths within the pipe scan enables classifying them generally into these 3 groups. The exact boundary locations of the groups can be a matter of discussion. However, a possible approach for establishing the boundaries is with the mean (μ) and standard deviation (σ) of the normal distribution fit to the wall loss data. In practice, for a real corroded pipe, it is difficult to assign a single level of average corrosion that occurs over its surface. Rather a range of average corrosion is appropriate as schematised in Figure 6. It is suggested that the range of average corrosion damage be defined from the distribution of the wall loss data as $(\mu - \sigma) < c \leq (\mu + \sigma)$. Similarly, the range of low corrosion damage and high corrosion damage can be defined as $0 \leq c \leq (\mu - \sigma)$ and $c > (\mu + \sigma)$ respectively.
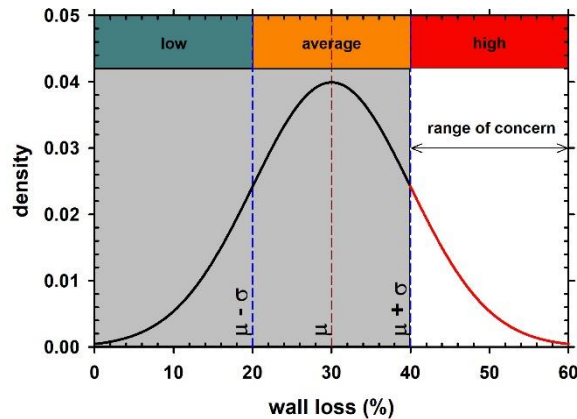
Figure 6. The wall loss distribution observed in a typical pipe scan can be classified into 3 groups as shown.

Following these classifications, it is clear that the region of concern for integrity analysis are those consisting of the high corrosion damage pits, *i.e.*, $> (\mu + \sigma)$. Consequently, it is suggested that the $(\mu + \sigma)$ be adopted as the threshold level to be applied for pipe wall-thickness scans. This will result in masking out the low and average pits from the analysis. This approach would also imply that the nominal wall thickness is corrected in any subsequent analysis with the threshold level.

Figure 7 illustrates some selected wall loss data from wall-thickness pipe scans of a water main, together with normal distribution fits. To demonstrate the usefulness of the thresholding methodology suggested, data from Figure 7c is taken as an example. Wall loss analysis at this location indicates that the μ and σ are 32.2% and 12.7% respectively, resulting in a threshold level of 44.9%.
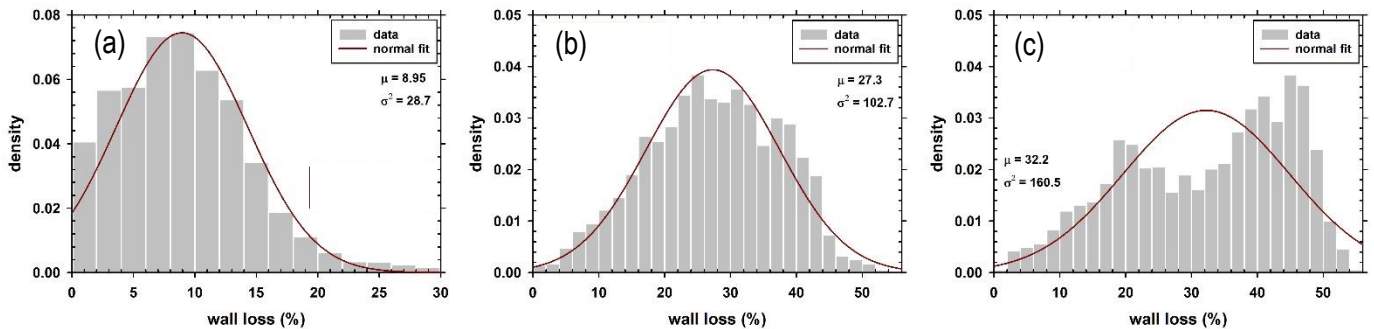

Figure 7. Normal distribution fit to the wall loss data from three pipe wall-thickness scans.

Figure 8 demonstrates the results of applying different threshold levels to the pipe scan data acquired from Figure 7c. The raw pipe scan shows several defects scattered over different regions of the scanned area. Application of a 20% threshold, which is usually used, does not improve in segmenting the critical elliptical corrosion patches. Similar problem exists if a threshold level of 32.2%, which is the mean of the normal distribution fit to the data shown in Figure 7c, is used. However, a practical segmentation is achieved upon using a threshold of $(\mu + \sigma) = 44.9\%$ and a critical elliptical corrosion patch geometry can be segmented. This demonstration provides confidence that the thresholding methodology suggested in this paper is worthwhile to pursue, especially since it binds well with the concept of corrosion progression and characteristics summarised in Figure 6.
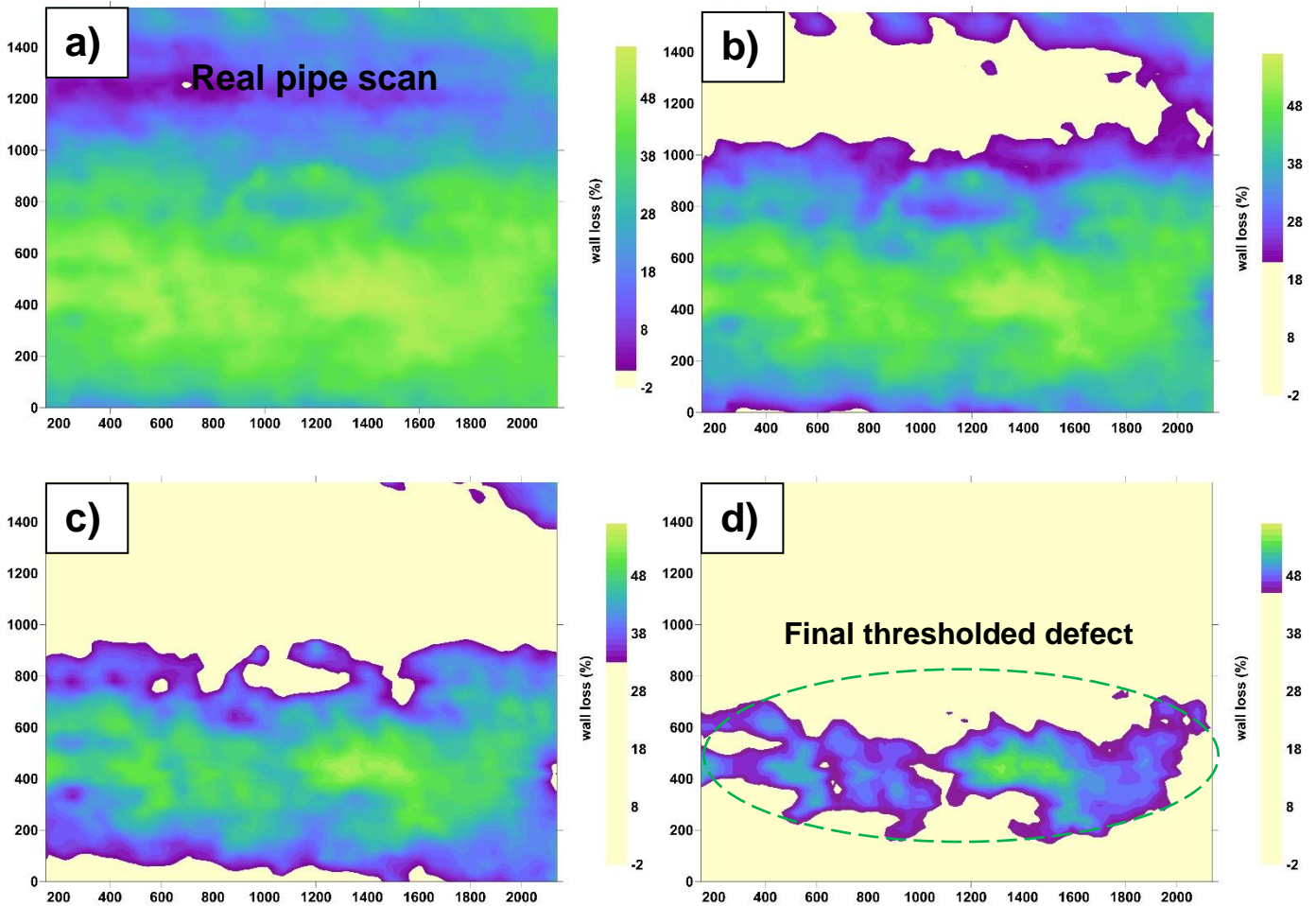
Figure 8. The original pipe scan data from Figure 7c shown in (a) was subjected to threshold levels of b) 20%, c) 32.2% (μ), and d) 44.9% (μ + σ). Application of threshold level set at (μ + σ) = 44.9% enables segmenting the familiar elliptical corrosion patch geometry (green dashed line) from the scan. Note that the defects circumscribed within the elliptical outline are continuous and therefore constitute one ellipse.

Summary workflow

1. Obtain the normal distribution fit to the wall loss data and determine its μ and σ. Set the threshold level at $(\mu + \sigma)\%$.

2. Apply the threshold level to the pipe scan data to segment critical elliptical corrosion patch and determine its dimensions $(2a, 2b, c)$.

3. Correct the nominal wall thickness (T_n) by the threshold level as per $T_{corr} = [1 - (\mu + \sigma)]T_n$, where T_{corr} is the corrected wall thickness.

4. Utilise the critical elliptical corrosion patch dimensions and corrected wall thickness in stress analysis.

It is acknowledged that in some instances other probability distribution functions may yield a better fit to the wall loss data than the normal distribution. It is suggested that the suitability of normal distribution fit to the wall loss data is randomly checked as a means of quality control. It is also emphasised that the concept presented here is a working solution that will need to be stringently validated with additional data. It is currently being investigated further by Monash.

1.3 Remaining Life Prediction/Time to Failure

1.3.1 Time to Failure due to Corrosion

For a cast iron pipe with some existing corrosion damage, the corrosion process will continue over time, leading to a growing corrosion defect. Considering an initial corrosion defect with dimensions $(2a_0, 2b_0, c_0)$, and a lateral extension rate and a radial corrosion rate of r_{sh} and r_{sv}, respectively. After n years, the dimensions of the corrosion patch will increase to $(2a_n, 2b_n, c_n)$ as shown in Figure 9.

Current patch

After n years

$(2a_0, 2b_0, c_0)$

$a_n = a_0 + r_{sh} \times n$

$b_n = b_0 + r_{sh} \times n$

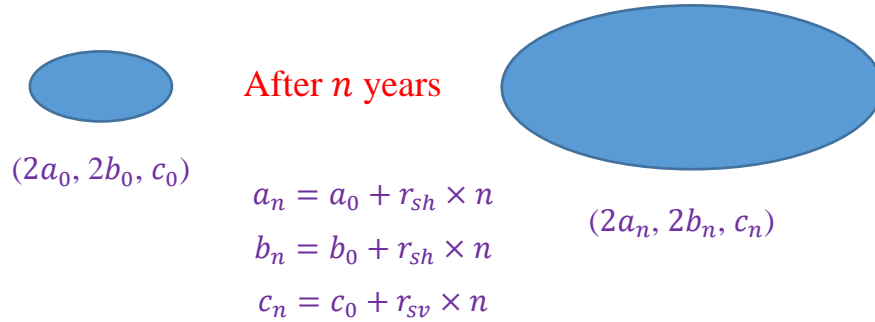$c_n = c_0 + r_{sv} \times n$

$(2a_n, 2b_n, c_n)$

Figure 9. Change of the patch dimensions over time

Let the maximum stress σ_{max} for the corrosion patch with dimensions $2a_n, 2b_n$ and c_n equals to the tensile strength of the cast iron material σ_t

$$\sigma_{max}(2a_n, 2b_n, c_n, other\ parameters) = \sigma_t \tag{4}$$

Then the number of years n can be calculated. When $\sigma_{max} = \sigma_t$, the number of years (n) is termed n_c and is the time to leak (years). The dimensions of the critical corrosion patch are considered to be $2a' = 2a_{n_c}$, $2b' = 2b_{n_c}$ and $c' = c_{n_c}$.

It should be noted that if b_n>250 mm, b_n is considered to take a value of 250mm. This assumption was made based on the field observation that corrosion patches formed by a cluster of corrosion pits generally have a patch width of no more than 500 mm.

1.3.2 Critical crack length

For a cast iron pipe with a longitudinal through-wall crack under internal pressure, the pipe internal diameter and wall thickness are D and T respectively, while the crack length is L (Figure 10). The stress intensity factor at the crack tip can be expressed as follows (Tada *et al.* 2000)

$$K_I = \frac{P_{max}D}{2T}\sqrt{\pi\frac{L}{2}} \cdot F(\lambda) \tag{5}$$

where K_I is the Mode I stress intensity factor, λ is defined as $\lambda = \frac{\sqrt{2}L}{2\sqrt{DT}}$ and $F(\lambda)$ can be expressed as follows

$$F(\lambda) = (1 + 1.25\lambda^2)^{1/2} \quad 0 < \lambda \leq 1$$
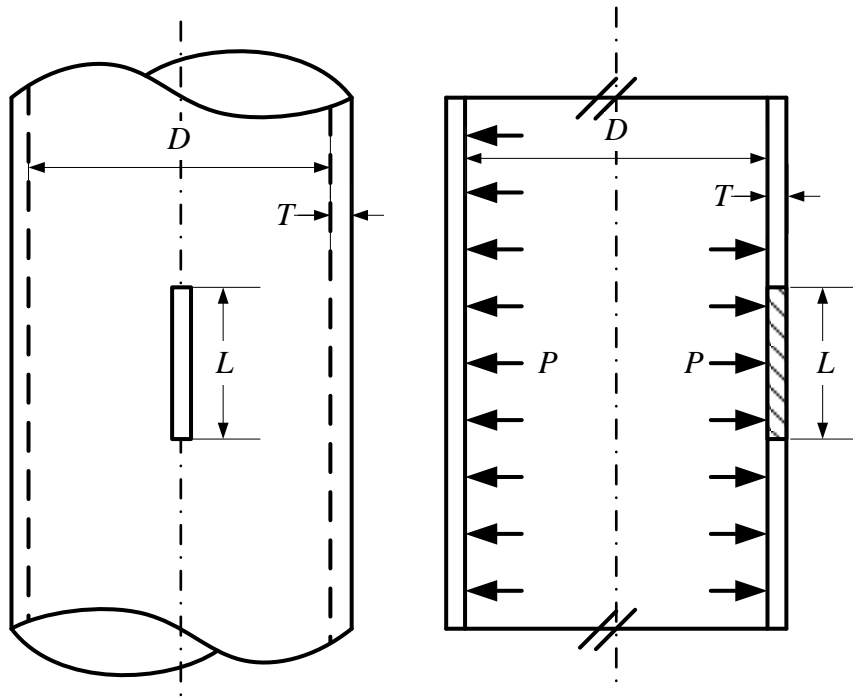$$F(\lambda) = 0.6 + 0.9\lambda \quad 1 \leq \lambda \leq 5 \tag{6}$$

Figure 10. A pressurized cast iron pipe with a through-wall crack (Adapted from Tada et al. 2000)

From Equation (5), it can be seen that the stress intensity factor K_I increases with the crack length L. When the stress intensity factor K_I reaches the fracture toughness K_{IC}, the corresponding crack length L is the critical crack length L_c.

It should be noted that the failure of the pipe due to corrosion could be either a "Leak" or a "Burst/Break". The failure type is determined here by comparing the critical patch length $2a'$ and the critical crack length L_c. If the critical patch length $(2a')$ is no smaller than the critical crack length (L_C), the pipe failure is considered to be a "Burst/Break". Otherwise, the pipe failure is considered to be a "Leak".

1.3.3 Leak to Break

Based on the "Time to Failure due to Corrosion", if the pipe only experiences a "Leak" rather than a "Burst/Break", further analysis can be conducted to assess the potential burst failure of corroded cast iron pipes caused by pressure transients. The "Leak to Break" considers the degradation of cast iron pipes caused by both corrosion and fatigue (pressure transients). The patch will grow over time due to corrosion while the crack formed when a leak occurs will grow sub-critically over time due to fatigue (pressure transients).

The crack growth rate is expressed as follows (Paris and Erdogan 1963)

$$\frac{d\left(\frac{L}{2}\right)}{dN} = C_f \Delta K^{m_f} \tag{7}$$

where L is the crack length, N is the number of fatigue cycles, C_f and m_f are the fatigue constants, ΔK is the change of stress intensity and can be expressed as follows

$$\Delta K(t) = K_{I,max}(t) - K_{I,min}(t) \tag{8}$$

$$K_{I,max}(t) = \frac{\sigma_{max}(P_{max}) + P_{max}D/(2T)}{2}\sqrt{\pi a} \cdot F(\lambda) \tag{9}$$

$$K_{I,min}(t) = \frac{\sigma_{min}(P_{min}) + P_{min}D/(2T)}{2}\sqrt{\pi a} \cdot F(\lambda) \tag{10}$$

where σ_{max} and σ_{min} are the maximum and minimum stress in the corroded cast iron pipe induced by the corrosion patch, respectively, P_{max} and P_{min} are the maximum and minimum internal pressure, respectively.

1.4 Pipe Failure Probability

The theoretical background of the probability of failure analysis for corroded pipes is briefly introduced below.

1.4.1 Instantaneous probability of failure (hazard rate)

The instantaneous probability of failure refers to the failure probability of an individual pipe at the current state (instant of time, t). The state parameters x are a vector of the pipe physical properties such as operating water pressure, pipe material strength, pipe configurations, etc. At time t, suppose the limit state of pipe failure is governed by a limit state function (LSF)

LSF: $g(x, t) = 0$

Then, the pipe failure occurs when $g(x, t) < 0$, and vice versa.

The instantaneous probability of failure is

$$P_f(t) = P_f[g(x, t) < 0] \tag{11}$$

where x is a vector of state parameters, each of which is uncertain with a statistical distribution. This equation can be evaluated by Monte Carlo simulation or first order reliability method. In the Pipe Failure Probability, the engineering reliability method is employed.

In engineering lifetime reliability theory, $P_f(t)$ is also called hazard rate.

1.4.2 Lifetime decay curves

Two decay curves will be given:

- Instantaneous (hazard rate): This curve is simply obtained by iteratively computing the $P_f(t)$ at some instants, such as with a 5-year interval.

- Cumulative: This curve is corresponding to the well-known reliability function, or cumulative distribution function of lifetime $F_T(t)$. At lifetime t, the following relationships hold:

$$F_T(t) = P_f(T_{LT} < t) \tag{12}$$

where T_{LT} is the lifetime of the pipe.

$$P_f(t) = f(t)/[1 - F_T(t)] \tag{13}$$

where $f(t)$ is the probability density function

$$F_T(t_i + 1) = F_T(t_i) + [1 - F_T(t_i)]P_f(t_i)(t_{i+1} - t_i) \tag{14}$$

By these equations ((12),(13) and (14)), the cumulative decay curve is directly derived from the instantaneous curve.

- Mean remaining lifetime (MRL): Suppose a pipe has survived to its current lifetime t, the expected remaining lifetime of the pipe can be calculated, by using the probability of failure and/or decay curves. The mean remaining lifetime is given by the following integral:

$$\mu(T_r) = E[t - T_r | t > T_r] = \left\{ \int_{T_r}^{\infty} [1 - F(x)]dx \right\}/[1 - F(T_r)] \tag{15}$$

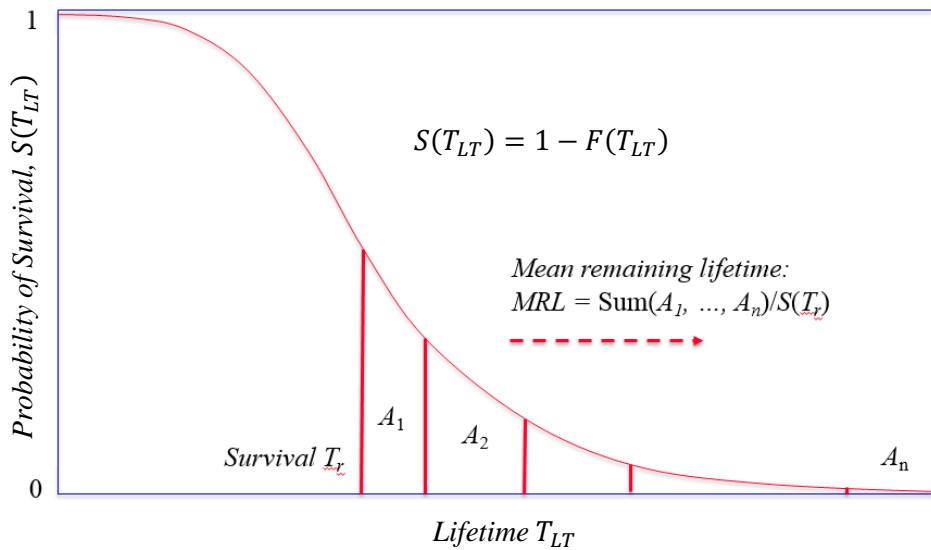A numerical solution is shown in the figure below (Figure 11).

Figure 11. Numerical solution to the mean remaining lifetime.

1.4.3   Lifetime decay curves as a result of corrosion deterioration

The lifetime decay curves are a function of the lifetime T_{LT}. At a single instant of lifetime, t, the hazard rate $P_f(t)$ and cumulative function $F_{T_{LT}}(t)$ are evaluated as mentioned above. For a period of pipe remaining lifetime T_{LT} from the current state (at time t_0) to the predicted state (at time t_p), which is divided into different points t_i ($i = 1, 2, ..., p - 1$) in time given a certain time interval, the corrosion model governs the deterioration of the pipe, by constantly increasing the dimensions of the corrosion patch and hence increasing the working stress in the surrounding area. This process is reflected in the equation $g(x, t) = 0$. As a result, the limit state function $g(x, t_i)$ at each interval instance t_i is different, although all the state parameters x have been assumed time-independent. This is why the decay curves show an increasing probability of failure trend over the pipe lifetime.

The flowchart (Figure 12) briefly illustrate the process of the probability of failure analysis (Ji *et al.* 2017).
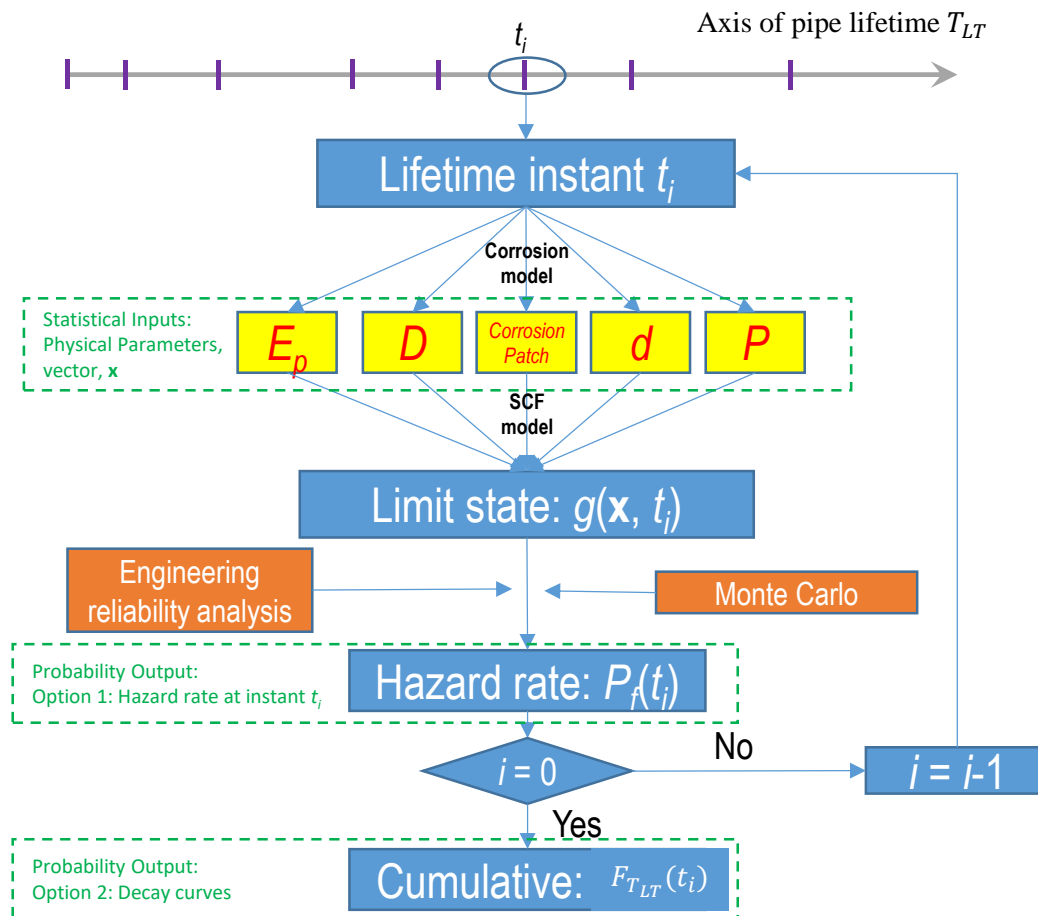
*Figure 12. Flowchart of the probability of failure analysis*

For lifetime probability of failure analysis, the probabilistic prediction decay curves are first produced using Monte Carlo simulations based on the statistical information of key parameters in Equations (1), (2) and (3) and failure mechanism of the pipe. Typical probabilistic decay curves were produced for a corroded cast iron pipe and shown in Figure 13(a). Then calibration is conducted to incorporate the past failures to determine the time of corrosion initiation, also known as the honeymoon period. This is achieved by adjusting the time of corrosion initiation to align the predicted failures with the recorded failures, i.e., by moving the decay curves along the time axis (Figure 13(b)). After calibration, the number of failures per year (failure rate) of the pipe section may be predicted using the probabilistic prediction decay curves, for a pipe section that consists of a number of pipe spools. Figure 13(c) presents the number of failures for the remaining lifetime of the pipe section.
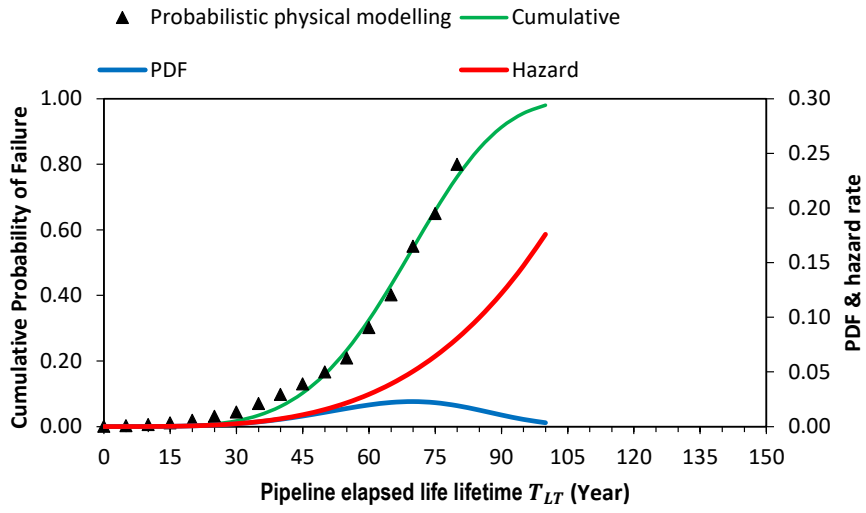
(a)
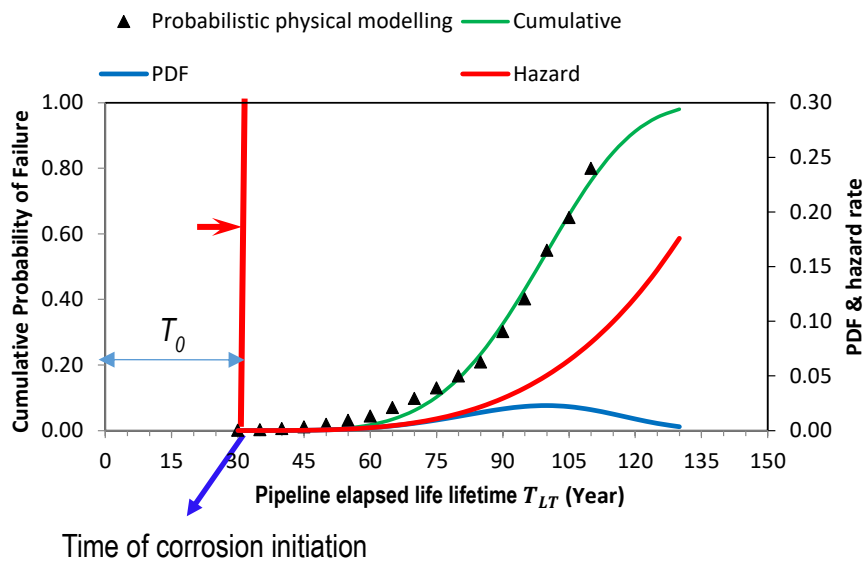
(b)
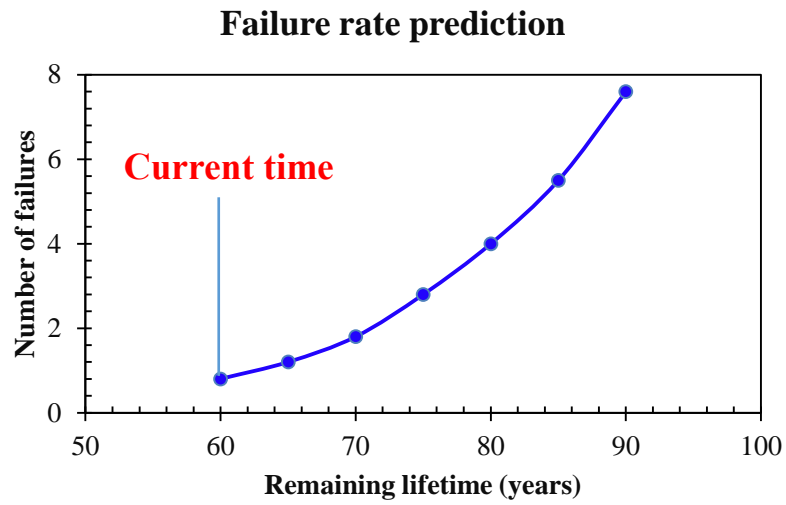
(c)

Figure 13. Procedure of the lifetime probability of failure by adjusting the time of corrosion initiation (a) Probabilistic prediction decay curves; (b) Calibration to incorporate past failures; (c) Pipe section failure rate prediction

NOTATION

$2a$	Patch length (mm)
$2a'$	Critical patch length (mm)
$2b$	Patch width (mm)
$2b'$	Critical patch width (mm)
c	Patch depth (mm)
c'	Critical patch depth (mm)
c_s	Intercept parameter for long-term corrosion of metallic pipes (mm)
C_f	Fatigue constant for host pipe under cyclic surge pressure
d	Initial hole (defect) size (mm)
D	Pipe internal diameter (mm)
D_0	Pipe external diameter (mm)
D_M	Mean diameter of the host pipe (mm)
DN	Pipe nominal diameter (mm)
E_p	Modulus of elasticity of host pipe material (GPa)
E_s	Soil modulus (MPa)
g	Acceleration due to gravity (m/s^2)
h	Pressure head (m)
H	Burial depth (mm)
H_w	Groundwater depth (mm)
k	Lateral earth pressure coefficient
k_1	Patch factor
k_2	Aspect ratio
K	Enhancement factor
K_{IC}	Fracture toughness of host pipe material (MPa m$^{1/2}$)
L_c	Critical crack length (mm)
L_p	Length of the pipe (m)
L_{ps}	Length of the pipe spool (m)
m_f	Fatigue constant for host pipe under cyclic surge pressure
$MAOP$	Maximum allowable operational pressure (MPa)
n_f	Cyclic surge factor
n_{PC}	Number of recurring cyclic surge pressure cycles per day
n_{TPC}	Total number of surge pressure cycles for the service life of pipe/lined pipe
N	Safety factor for host pipe
P	Operating pressure (MPa)
P_G	Groundwater load (MPa)
P_{GC}	Groundwater load capacity (MPa)
PN	Nominal pressure (bar)

P_N	External pressure on the liner (MPa)
P_T	Test pressure (MPa)
P_c	Recurring cyclic surge pressure (MPa)
P_{max}	Maximum allowable pressure (MPa)
P_{min}	Minimum internal pressure (MPa)
P_s	Surge pressure (MPa)
P_v	Vacuum pressure (MPa)
q_t	Total external pressure on pipes (MPa)
q_{tc}	Liner capacity for total external pressure (MPa)
r_s	Minimum corrosion rate (long-term) of metallic pipes (mm/y)
r_{sh}	Lateral extension rate for metallic pipes (mm/y)
r_{sv}	Radial corrosion rate for metallic pipes (mm/y)
SCF	Stress concentration factor
SCF'	Critical stress concentration factor
t	Time (years)
T	Pipe wall thickness allowing for uniform corrosion (mm)
T_{ext}	Estimated external uniform corrosion (mm)
T_f	AC pipe remaining wall thickness at failure (mm)
T_{int}	Estimated internal uniform corrosion (mm)
T_L	Liner thickness (mm)
T_n	Pipe nominal wall thickness (mm)
W	Traffic load (kN)
W_s	Live load (MPa)
α	Coefficient of thermal expansion/contraction (mm/mm/°C)
β	Fraction of liner service life when out of service
γ_s	Soil unit weight (kN/m³)
γ_w	Unit weight of water (kN/m³)
ΔT	Temperature change (°C)
ν_p	Poisson's ratio of host pipe material
σ_p	Tensile stress in the host pipe (for AC pipe) (MPa)
$\sigma_{t,AC}$	Ultimate tensile strength of AC (MPa)
σ_t	Ultimate tensile strength of host pipe material (MPa)
σ_y	Yield strength of steel (MPa)
τ	Transition period between short-term and long-term corrosion (y)
Φ	Soil friction angle (°)

DISCLAIMER

1. Use of the information and data contained within the Pipe Failure Analysis Module is at your sole risk.

2. If you rely on the information in the Pipe Failure Analysis Module, then you are responsible for ensuring by independent verification of its accuracy, currency, or completeness.

3. The information and data in the Pipe Failure Analysis Module is subject to change without notice.

4. The Pipe Failure Analysis Module developers may revise this disclaimer at any time by updating the Pipe Liner Selection Module.

5. Monash University and the developers accept no liability however arising for any loss resulting from the use of the Pipe Failure Analysis Module and any information and data.

CONCLUSIONS

This document provided the theory of the Pipe failure analysis used in the Pipe Evaluation Platform. This model was originally developed for cast iron pipes, if adjusted for other metallic pipes such as mild steel or ductile iron, the user must proceed with caution. Further research needs to be conducted to verify the pipe failure analysis for other metallic pipes.

REFERENCES

Anderson, T.L. (2005). Fracture mechanics fundamentals and applications. CRC Press Taylor and Francis Group, Florida.

ASME B31 (2012). Manual for determining the remaining strength of corroded pipelines: A supplement to ASME B31 code for pressure piping. *In* ASME B31. American Society of Mechanical Engineers, American National Standards Institute.

ASTM G46-94 (2005). Standard guide for examination and evaluation of pitting corrosion. *In* ASTM G46-94. ASTM International, West Conshohocken, PA, USA.

Deo, R.N., Rathnayaka, S., Zhang, C., Fu, G.Y., Shannon, B., Wong, L., and Kodikara, J.K. (2019). Characterization of corrosion morphologies from deteriorated underground cast iron water pipes. *Materials and Corrosion*, **70**(10): 1837-1851.

Fu, G., Zhang, C., Deo, R., Rathnayaka, S., Shannon, B., and Kodikara, J. (2020). A model of stress concentration factors for external corrosion patches on large-diameter underground cast iron pipes. *Sustainable and Resilient Infrastructure*: 1-12.

Ji, J., Robert, D.J., Zhang, C., Zhang, D., and Kodikara, J. (2017). Probabilistic physical modelling of corroded cast iron pipes for lifetime prediction. *Structural Safety*, **64**: 62-75.

Kodikara, J. (2018). Advanced Condition Assessment and Failure Prediction Technologies for Optimal Management of Critical Water Supply Pipes, The Water Research Foundation.

Paris, P., and Erdogan, F. (1963). A Critical Analysis of Crack Propagation Laws. *Journal of Basic Engineering*, **85**(4): 528–533.

Pilkey, W.D., and Pilkey, D.F. (2008). Peterson's stress concentration factors. John Wiley & Sons.

Robert, D.J., Rajeev, P., Kodikara, J., and Rajani, B. (2016). Equation to predict maximum pipe stress incorporating internal and external loadings on buried pipes. *Canadian Geotechnical Journal*, **53**(8): 1315–1331.

Tada, H., Paris, P.C., and Irwin, G.R. (2000). The stress analysis of cracks handbook. ASME, New York.

Zhang, C., Rathnayaka, S., Shannon, B., Ji, J., and Kodikara, J. (2017). Numerical interpretation of pressurized corroded cast iron pipe tests. *International Journal of Mechanical Sciences*, **128-129**: 116-124.